City Research Online

City St George's, University of London

Citation: Mergos, P.E. & Kappos, A.J. (2012). A gradual spread inelasticity model for R/C beam-columns, accounting for flexure, shear and anchorage slip. ENGINEERING STRUCTURES, 44, pp. 94-106. doi: 10.1016/j.engstruct.2012.05.035

This is the submitted version of the paper.

This version of the publication may differ from the final published version. To cite this item please consult the publisher's version.

Permanent repository link: https://openaccess.city.ac.uk/id/eprint/3561/

Link to published version: https://doi.org/10.1016/j.engstruct.2012.05.035

Copyright and Reuse: Copyright and Moral Rights remain with the author(s) and/or copyright holders. Copies of full items can be used for personal research or study, educational, or not-for-profit purposes without prior permission or charge, unless otherwise indicated, provided that the authors, title and full bibliographic details are credited, a hyperlink and/or URL is given for the original metadata page and the content is not changed in any way. For full details of reuse please refer to City Research Online policy.

City Research Online: http://openaccess.city.ac.uk/ publications@citystgeorges.ac.uk

*Manuscript
Click here to view linked References

A gradual spread inelasticity model for R/C beam-columns, accounting for flexure, shear and anchorage slip

Panagiotis E. Mergos, Andreas J. Kappos*

Laboratory of Concrete and Masonry Structures, Department of Civil Engineering, Aristotle University of Thessaloniki, Thessaloniki 54124, Greece

Abstract. *A new beam-column model is developed for the seismic analysis of reinforced concrete (R/C) structures. This finite element consists of two interacting, gradual spread inelasticity sub-elements representing inelastic flexural and shear response and two rotational springs at the ends of the member to model anchorage slip effects. The flexural sub-element is able to capture gradual spread of flexural yielding in plastic hinge regions of R/C members. The shear sub-element interacts throughout the analysis with the flexural sub-element, in the location of the plastic hinge regions, in order to capture gradual spread of inelastic shear deformations as well as degradation of shear strength with curvature ductility demand based on an analytical procedure proposed herein. The skeleton curves and hysteretic behaviour in all three deformation mechanisms are determined on the basis of analytical procedures and hysteretic models found to match adequately the experimental results. Empirical formulae are proposed for the shear distortion at onset of stirrup yielding and onset of shear failure. The proposed element is implemented in the general finite element code for damage analysis of R/C structures IDARC and is validated against experimental results involving R/C column and frame specimens failing in shear subsequent to yielding in flexure. It is shown that the model can capture well the hysteretic response and predict reliably the type of failure of these specimens.*

Keywords: Reinforced concrete; finite elements; beam-column element; gradual spread; shear-flexure interaction; bond-slip.

1 Introduction

Seismic response analysis of reinforced concrete structures requires realistic analytical models that can predict strength, stiffness and ductility characteristics of members under cyclic loading. The current state of the art in mathematical modelling of reinforced concrete behaviour permits reasonably accurate predictions of hysteretic response in flexure. However, inelastic deformations

* Corresponding author. Tel.: +30 2310 995743; Fax: +30 2310 995614.
E-mail address: ajkap@civil.auth.gr

generated during seismic response are by no means limited to flexure. Experimental investigations have indicated that inelastic shear distortions can be significant in local areas, such as hinging regions, even when the overall behaviour is governed by flexure [1-4]. Moreover, it has been well documented [5-7] that an R/C member may fail in shear due to interaction with flexure despite the fact that it has been provided initially with shear capacity greater than the one corresponding to yielding in flexure.

Several researchers have attempted to explicitly include inelastic shear response in assessment of R/C structures [8-13]. Typically, in these studies, shear rigidity is assumed to be constant along the concrete member or shear deformations developed along the entire element are lumped in inelastic rotational or translational springs placed at the ends of the member. The former approach cannot be exact due to interaction of shear and flexural deformations occurring in the plastic hinge regions. The latter approach can be accurate only in the special case where the moment distribution along the member is already known and the point of contraflexure remains fixed throughout the analysis.

Additionally, a number of fibre elements have been developed incorporating the shear flexibility effect. In these models, shear deformations are either uncoupled [13] or coupled [12] with axial and bending effects at the section level. Nevertheless, the computational effort involved, especially in the latter case, limits their feasibility for response history analysis of complete multi-storey structures. Furthermore, the Gauss or Gauss-Lobatto integration technique used in these elements does not represent, in an exact manner, the actual phenomenon, when inelastic deformations tend to spread gradually from the member ends to the midspan.

To capture the gradual spreading phenomenon, a spread inelasticity formulation has to be developed. A number of researchers have introduced flexural, spread inelasticity elements [9,14,15]. The writers [16-18] have developed a shear spread inelasticity element for the case where shear force varies along the member due to distributed loading. No model has been developed so far to reproduce gradual spread of inelastic shear deformations following progressive growth of the plastic hinges towards the midspan.

In most cases, shear-flexure interaction effect is taken into consideration adopting advanced analytical procedures like the modified compression field theory (MCFT) [19]. These methods, albeit conceptually attractive, have not yet been extended to cope successfully with degradation of shear strength in plastic hinges and cyclic loading effects [20]. Additionally, the computational effort required hinders their application in seismic analysis of complex R/C structures.

A number of analytical models [10,13], applied shear strength models (e.g. Priestley et al. [5]) to capture degradation of shear strength with increasing flexural ductility demand. While these models are able to predict shear failure with a reasonable accuracy, they have not been developed with a view to reproducing rapid development of shear deformations, following flexural yielding. Hence, the need arises for a simple analytical procedure which will provide reasonably accurate predictions of shear strength and deformations, especially in the yielded end-regions of R/C members.

Existing beam-column elements considering separately shear deformations, with the exception of the analytical models presented in [9,11], do not account for anchorage slip effects in an explicit manner. Fixed-end rotations caused by anchorage slip may influence significantly the stiffness and deformation capacity of R/C members, while they have not yet been related experimentally to degradation of shear strength. Moreover, fixed end rotations are treated only as a function of the moments acting at the ends of the member, i.e. not of the bending moment diagram distribution, which determines variation of flexural deformations along the member. Hence, it is evident that ignoring bond-slip effects or lumping them together with flexural deformations inside a single end rotational spring may lead an analytical model to erroneous results.

The goal of the present study is to develop a cost-efficient beam-column model, suitable for seismic analysis of complex R/C frame structures, which, at the same time, will be capable of taking into account rather complex mechanisms, such as gradual spread of inelastic flexural and shear deformations from the member ends to the midspan, degradation of shear strength with curvature ductility demand, coupling between inelastic flexural and shear deformations in the plastic hinges, and fixed-end rotations caused by anchorage slip.

With the objective to verify the capabilities of the proposed model to reproduce the aforementioned mechanisms, the results of the analytical model are compared with those experimentally obtained from a number of well-documented tests of R/C column and frame specimens exhibiting rather complex behaviour i.e. failing in shear after yielding in flexure. Whenever possible, the comparisons are not restricted to total response parameters, but also encompass individual deformation components (curvatures, distortions, anchorage slip fixed-end rotations), with a view to verifying individual features of the model.

2 Finite element formulation

The proposed, member-type, finite element is based on the flexibility approach (force-based element) and belongs to the class of phenomenological models. It consists of three sub-elements representing flexural, shear, and bond-slip response (Fig. 1). The total flexibility matrix (F) is calculated as the sum of the flexibilities of its sub-elements and can be inverted to produce the element stiffness matrix (K). Hence:

$$F = F^{fl} + F^{sh} + F^{sl} \quad (1)$$

$$K = F^{-1} \quad (2)$$

Where, F, F^{fl}, F^{sh}, F^{sl} are the basic total, flexural, shear and anchorage slip, respectively, tangent flexibility matrices. K is the basic tangent stiffness matrix of the element, relating incremental moments ΔM_A, ΔM_B and rotations $\Delta\theta_A$, $\Delta\theta_B$ at the ends A and B of the flexible part of the element (Fig. 1) through the following equation

$$\begin{bmatrix} \Delta M_A \\ \Delta M_B \end{bmatrix} = K \cdot \begin{bmatrix} \Delta \theta_A \\ \Delta \theta_B \end{bmatrix} \quad (3)$$

The local stiffness matrix, relating displacements and forces at the element joints, is then easily determined following standard structural analysis procedures. The components of the aforementioned finite element, as well as their interaction, are described in the following sections.

3 Flexural sub-element

This sub-element (Fig. 1c) is used for modelling the flexural behaviour of an R/C member subjected to cyclic loading before, as well as after, yielding of longitudinal reinforcement. It consists of a set of rules governing the hysteretic moment-curvature (M-φ) response of the member end sections, and a spread inelasticity model describing flexural stiffness distribution along the entire member.

3.1 M-φ relationship for member end-sections

The M-φ relationship at each end section of the member is described by the primary curve and the rules determining its hysteretic behaviour. The primary M-φ relationship is derived using standard flexural analysis and appropriate bilinearization of the resulting curve.

Loading response is assumed to follow the bilinear envelope curve. Unloading is based on the respective Sivaselvan & Reinhorn [21] hysteretic rule adjusted for mild stiffness degradation characterising flexural response. This is achieved by setting the unloading parameter of this hysteretic model equal to 15. Reloading aims at the previous point of maximum excursion in the opposite direction [22].

3.2 Flexural spread inelasticity model

The flexural spread inelasticity model presented herein is based primarily on the respective one by Soleimani et al. [14]. The stiffness distribution along the member is assumed to have the shape shown in Fig. 2, where: L is the length of the member; EI_A and EI_B are the current flexural rigidities of the sections at the ends A and B, respectively; EI_o is the stiffness of the intermediate part of the element; α_A and α_B are the yield penetration coefficients. The flexural rigidities EI_A and EI_B are determined from the M-φ hysteretic relationship of the corresponding end sections. For simplicity, in this study, it is assumed that the state (loading, unloading, reloading) and the stiffness of the spread plastic zone is controlled by the state and stiffness of the section at the end of the member.

The yield penetration coefficients specify the proportion of the element where the acting moment exceeds the end-section yield moment. These coefficients are first calculated for the current moment distribution from Eqns. (4)-(5), where M_{yA} and M_{yB} are the respective flexural yielding moments of end sections A and B. Then, they are compared with the previous maximum penetration lengths; the yield penetration lengths cannot be smaller than their previous maximum values.

$$\alpha_A = \frac{M_A - M_{yA}}{M_A - M_B} \leq 1 \quad (4)$$

$$\alpha_B = \frac{M_B - M_{yB}}{M_B - M_A} \leq 1 \quad (5)$$

Having established the stiffness distribution along the R/C member at each step of the analysis, the coefficients of the flexibility matrix of the flexural sub-element can be derived from closed-form analytical expressions [14], by applying the principle of virtual work.

4 Shear sub-element

The shear sub-element (Fig. 1d) represents the hysteretic shear behaviour of the R/C member prior and subsequent to shear cracking, flexural yielding, and yielding of the shear reinforcement. Herein, this sub-element has been designed in a similar way to the flexural element described above. It consists of a set of rules determining V-γ (shear force vs. shear strain) hysteretic behaviour of the member end and intermediate regions, and a shear spread inelasticity model determining distribution of shear stiffness along the R/C member.

Shear hysteresis is determined by the V-γ skeleton curve and a set of rules describing response during unloading and reloading. The primary curve is first derived without considering shear-flexure interaction effects. Then, by applying an appropriate procedure proposed in this study, the shear-flexure interaction effect is taken into consideration at the locations of plastic hinges.

4.1 V-γ envelope curve without shear-flexure interaction

The initial V-γ primary curve (Fig. 3) is independent from flexure and is used to model shear hysteresis outside the plastic hinge regions for members that have yielded in flexure or the response of the entire element for members that have not yielded in flexure.

The V-γ primary curve consists of four branches, but has only three different slopes, as explained later on. The first branch, with uncracked stiffness GA_o, connects the origin and the shear cracking point, which is defined as the point where the nominal principal tensile stress exceeds the tensile strength of concrete. Shear force at cracking V_{cr} is calculated by adopting an analytical procedure suggested by Sezen and Moehle [7].

The second and third branches of the initial primary curve have the same slope and connect the shear cracking point with the point corresponding to the onset of yielding of transverse reinforcement, or else the point of attainment of maximum shear strength (V_{uo}, γ_{st}). These branches are separated at the point corresponding to flexural yielding (V_y, γ_y). This approach is adopted in order to distinguish hysteretic shear behaviour before and after flexural yielding [4].

To estimate shear strength V_u, the approach proposed by Priestley et al. [5] is invoked. According to this approach, V_u is given by

$$V_u = k \cdot \sqrt{f_c} \cdot \left(0.80 A_g\right) + N \cdot \tan a + \frac{A_{sw} \cdot f_{yw} \left(d - d'\right) \cdot \cot \theta}{s} \qquad (6)$$

wherein A_{sw} is the area of transverse reinforcement oriented parallel to shear force; f_c is the concrete compressive strength; f_{yw} is the yield strength of transverse reinforcement; d-d' is the distance measured parallel to the applied shear between centres of longitudinal reinforcement; s is the spacing of transverse reinforcement; θ is the angle defined by the column axis and the direction of the diagonal compression struts; k is a parameter depending on the curvature ductility demand as shown in Fig. 4, and α is the angle formed by the column axis and the line joining the centres of the flexural compression zones at the top and bottom of the column. For the initial primary curve, V_{uo} is derived by setting in Eq. (6) the value of k corresponding to $\mu_\varphi \leq 3$ (i.e. no strength degradation).

The stiffness of the second and third branches, GA_1, which represent shear deformation γ_s caused by shear force V_s in a cracked member, can be estimated by Eq. (7) derived by the truss analogy approach [23]

$$GA_1 = \frac{\Delta V_s}{\Delta \gamma_s} = \frac{E_s \cdot b \cdot \left(d - d'\right) \cdot \rho_w \cdot \sin^4 \theta \cdot \cot^2 \theta}{\sin^4 \theta + \eta \cdot \rho_w} \qquad (7)$$

where b is the section width; ρ_w is the volumetric ratio of transverse reinforcement; E_s is the modulus of elasticity of steel; $n=E_s/E_c$ is the modular ratio, and E_c is the concrete modulus of elasticity.

Shear distortion at onset of stirrup yielding γ_{st} can be easily determined by setting $\Delta V_s = V_w$ where V_w is the shear strength contributed by the transverse reinforcement. Although the aforementioned procedure is based on a rational approach, calibration studies by the writers showed that it does not account accurately enough for the influence of axial load and member aspect ratio on γ_{st}.

Regression analyses performed by the writers showed that best correlation with experimental results is achieved when, in calculating γ_{st} by the truss analogy approach, the angle θ is taken equal to 45^o (unless limited to larger angles by the potential corner-to-corner crack) and the derived value is then multiplied by two modification factors. The first modification factor κ takes into account the influence of the normalised axial load v and is given by Eq. (8), while the second modification factor λ represents the influence of the aspect ratio (shear span, L_s, divided by column depth, h) and is given by Eq. (9).

$$\kappa = 1 - 1.07 \cdot v \qquad (8)$$

$$\lambda = 5.37 - 1.59 \cdot \min\left(2.5, \frac{L_s}{h}\right) \qquad (9)$$

Hence, if γ_{truss} is the shear distortion at onset of stirrup yielding derived by the truss analogy approach, it is proposed herein that γ_{st} is given by the following equation.

$$\gamma_{st} = \kappa \cdot \lambda \cdot \gamma_{truss} \qquad (10)$$

The regression analyses are based on the experimental results for 16 R/C columns (Table 1). The experimental results involved average shear distortions along the length of pure shear critical R/C specimens or flexure-shear critical elements failing in shear immediately after flexural yielding. The values followed by asterisk were derived indirectly, using the respective procedure described in [16]. The mean, median and coefficient of variation of the ratios of the experimental over the predicted values are 0.99, 0.97 and 0.19 respectively. The coefficient of determination R^2 is 0.82.

Experimental studies [1, 24] have shown that R/C members critical in shear do not lose immediately their lateral strength after yielding of transverse reinforcement. This observation leads to the conclusion that shear strain γ_u corresponding to onset of shear failure may considerably exceed γ_{st}. For this reason, a horizontal branch is added to the envelope V-γ curve, for $\gamma>\gamma_{st}$, to model response after yielding of transverse reinforcement.

On the basis of experimental results for 25 R/C specimens (Table 1) failing in shear, the writers have developed an empirical formula correlating γ_u with the level of the applied axial load, the amount of transverse reinforcement and the member shear-span ratio L_s/h. Conservatively, it is assumed in this study that shear failure coincides with the onset of significant lateral strength degradation. The experimental results involved either measured shear strains in the vicinity of the plastic hinge regions for flexure-shear critical R/C members or average shear distortions along the length of pure shear critical R/C specimens or members failing in shear immediately after flexural yielding. For the average shear distortions along the member length, the values followed by an asterisk in Table 1 were derived indirectly, using the respective procedure described in [16]. The proposed relationship is

$$\gamma_u = \lambda_1 \cdot \lambda_2 \cdot \lambda_3 \cdot \gamma_{st} \geq \gamma_{st} \tag{11.1}$$

$$\lambda_1 = 1.0 - 2.5 \cdot \min\left(0.40, \nu\right) \tag{11.2}$$

$$\lambda_2 = \min\left(2.5, L_s / h\right)^{2.0} \tag{11.3}$$

$$\lambda_3 = 0.31 + 17.8 \cdot \min\left(\omega_\kappa, 0.08\right) \tag{11.4}$$

$$\omega_\kappa = \frac{A_{sw} \cdot f_{yw}}{b \cdot s \cdot f_c} \tag{11.5}$$

According to Eq. (11), the difference between γ_u and γ_{st} increases as the amount of transverse reinforcement and shear span ratio increase, and the normalised axial load decreases. The mean, median, and coefficient of variation of the ratios of the experimental over the predicted values are 1.00, 1.00 and 0.34. The coefficient of determination R^2 is 0.96.

It is important to note that the empirical formulae proposed herein for both γ_{st} and γ_u are based on a set of data (Table 1) satisfying the following criteria: $1.11 \leq L_s/h \leq 3.91$; $0 \leq \nu \leq 0.61$ and $0.47\% \leq \omega_\kappa \leq 8.13\%$; hence, they can only be applied with confidence for RC members that satisfy the aforementioned criteria.

4.2 V-γ envelope curve including shear-flexure interaction

Several studies [5-7] have demonstrated that shear strength degrades due to disintegration of the plastic hinge zones caused by inelastic flexural deformations. Furthermore, it has been shown experimentally [1-4] that shear distortions in the plastic hinge regions may increase rapidly ("shear-flexural yielding") subsequent to flexural yielding, despite the fact that shear force demand remains almost constant, as it is controlled by flexural yielding. The combination of these phenomena is defined in this study as shear-flexure interaction effect. It is shown here that both of these phenomena can be represented simultaneously by combining the shear strength model of Priestley et al. [5] and the truss analogy approach [23].

Fig. 5a illustrates the variation of the force carried by shear resisting mechanisms (concrete V_c and truss V_s) in the plastic hinge region of a single R/C column following the Priestley et al. [5] shear strength approach (for clarity of the figure, the contribution of axial load is lumped into V_c). It can be seen that, immediately after shear cracking, the truss contribution V_s increases, to meet additional shear force demand ΔV. This is the case even after flexural yielding and before μ_φ reaches the value of 3. However, after $\mu_\varphi=3$, V_s increases to accommodate both ΔV and additional deterioration of V_c; this means that, for the same ΔV, V_s increases now at a higher rate. On μ_φ reaching the value of 15, the concrete shear resisting mechanism V_c reaches its residual strength and consequently V_s increases again solely due to ΔV.

Since the shear strain γ_s subsequent to shear cracking is correlated with V_s via Eq. (7), variation of γ_s with increasing μ_φ can be easily extracted (Fig. 5b). From this figure, it can be seen that immediately after flexural yielding γ_s increases at a slow rate with increasing μ_φ. Nevertheless, after $\mu_\varphi=3$, increase of γ_s accelerates. After $\mu_\varphi=7$, γ_s continues to increase more rapidly than when $\mu_\varphi<3$ but less rapidly than when $3\leq\mu_\varphi\leq7$. Finally, when $\mu_\varphi>15$, γ_s continues to increase, but at the slow rate that initiated when $\mu_\varphi<3$.

Generalising the above, the shear strain increment $\Delta\gamma_s$ caused by a shear force increment ΔV, when shear-flexure interaction effect is taken into account, can be estimated from Eq. (11), where ΔV_s is the increment of the shear force resisted by the truss mechanism caused by the increment of the applied shear force ΔV and the additional drop of the shear capacity of the concrete shear resisting mechanism $\Delta degV_c$.

$$\Delta\gamma_s = \frac{\Delta V_s}{GA_1} = \frac{\Delta V + \Delta \deg V_c}{GA_1} \tag{11}$$

If GA_{eff} is the tangent stiffness of the shear primary curve including shear-flexure interaction effect, then it yields the same increment of shear distortions $\Delta\gamma_s$ only for the applied shear force increment ΔV (without $\Delta degV_c$), as illustrated in Fig. 6. Hence

$$\Delta\gamma_s = \frac{\Delta V}{GA_{eff}} \tag{12}$$

Combining Eqs. (11) and (12) and solving for GA_{eff}, the following equation is obtained

$$GA_{eff} = \frac{\Delta V}{\Delta V + \Delta \deg V_c} \cdot GA_1 \quad (13)$$

Eq. (13) shows that GA_{eff} can only be either equal to, or smaller than, GA_1. Equality holds only when the degradation of the concrete shear resisting mechanisms is negligible. Moreover, it is clear that GA_{eff} becomes a function of the shear force increment ΔV. But if it is to be applied in the analytical procedure, ΔV will be influenced by GA_{eff} as well, since the latter will affect the flexibility matrix of the element (as shown in §4.4). To resolve this issue, an iterative analytical scheme, applied at the respective load step of nonlinear analysis, is proposed herein.

According to this scheme, an initial value of GA_{eff} is assumed. Based on this shear rigidity, shear force increment ΔV and additional drop of the concrete shear resisting mechanism capacity $\Delta deg V_c$ for the examined member are evaluated. By applying these values in Eq. (13), a new value of GA_{eff} is calculated. The iterative procedure terminates, when the values of GA_{eff} converge with a pre-specified tolerance. Applying this procedure, it was found that numerical convergence is almost immediate. The number of iterations may increase as the influence of shear deformations on element flexibility increases, but the additional computational cost is justified by the significance of calculating accurately shear response in this case.

4.3 V-γ hysteretic model

Shear hysteresis is characterised by significant pinching effect, stiffness and strength deterioration. This behaviour is modelled using the proposals by Ozcebe and Saatcioglu [4] as a basis, with several modifications and improvements. Although, that hysteretic model was calibrated against experimental results and was found to yield a reasonable match, it has not been designed with a view to being incorporated in a dynamic nonlinear analysis framework. With this in mind, the writers have proposed specific modifications regarding both the unloading and reloading branches that can be found in their previous publication [16].

4.4 Shear spread inelasticity model

In §4.2, rapid increase of inelastic shear deformations inside plastic hinge regions has been explained. Following gradual growth of plastic hinge regions, inelastic shear strains tend to expand gradually from the member ends to the midspan. To capture this phenomenon, an innovative approach is adopted herein, based on the concept of gradual spread inelasticity models.

More specifically, a shear spread inelasticity model is proposed, having the shear stiffness distribution of Fig. 7c, where α_{As} and α_{Bs} are the "shear-flexural yield penetration" coefficients. These coefficients specify the proportion of the element where "shear-flexural yielding" has developed, triggered by flexural yielding as described in §4.2. Since "shear-flexural yielding" develops inside plastic hinge regions, it is reasonable to assume that

$$\alpha_{As} = \alpha_A \; ; \; \alpha_{Bs} = \alpha_B \tag{14}$$

In Fig. 7c, GA_A and GA_B are the current shear rigidities of the inelastic regions at the ends A and B, respectively. These values can be derived from the V-γ hysteretic relationships of the corresponding end sections, where the skeleton curves are determined including shear-flexure interaction effect (GA_{eff} in §4.2), based on the inelastic curvature demand of the respective end of the flexural sub-element. In the case of constant shear force examined here, the level of acting shear force and the loading state (loading, unloading and reloading) are the same for all sections within the inelastic shear zones. Consequently, it can be assumed, with reasonable accuracy, that shear stiffness distribution remains uniform within these regions.

Shear stiffness GA_M occurs in the intermediate (elastic) part of the element. It can be determined again by the V-γ hysteretic model, but by adopting a primary curve without assigning shear-flexure interaction effect, as described in §4.1. Similarly, it can be considered as uniform in the specific part of the element.

After determining the distribution of *GA* along the R/C member at each step of the analysis and by applying the principle of virtual work, the coefficients of the flexibility matrix of the shear sub-element are given by the following equation

$$f_{ij}^{sh} = \frac{a_{As}}{GA_A \cdot L} + \frac{1 - a_{As} - a_{Bs}}{GA_M \cdot L} + \frac{a_{Bs}}{GA_B \cdot L} \text{ (i,j=A,B)} \tag{15}$$

Based on the above, a dual coupling effect between the flexural and the shear sub-element is achieved. This effect determines both the length and stiffness of the inelastic zones of the shear sub-element allowing for constant monitoring of the gradual spread of inelastic shear strains from the member ends to the mid-span, with the minimum possible computational cost.

5 Anchorage slip sub-element

The bond-slip sub-element accounts for the fixed-end rotations which arise at the interfaces of adjacent R/C members due to bond deterioration and the ensuing slippage of the reinforcement anchorage in the joint regions. The proposed model consists of two concentrated rotational springs located at the member-ends; the two (uncoupled) springs are connected by an infinitely rigid bar (Fig. 1e). Following this formulation, the coefficients of the bond-slip flexibility matrix F^{sl} are given by Eq. (16), where f_A^{sl} and f_B^{sl} are the flexibilities of the concentrated rotational springs at the ends A and B respectively. These flexibilities depend on the moment - fixed end rotation (M-θ_{slip}) envelope curve and the model used to represent hysteretic behaviour of each rotational spring.

$$F^{sl} = \begin{bmatrix} f_A^{sl} & 0 \\ 0 & f_B^{sl} \end{bmatrix} \tag{16}$$

The M-θ_{slip} skeleton curve is derived on the basis of a simplified procedure [34,35] assuming uniform bond stress along different segments of the anchored rebar (Fig. 8). These segments are the

elastic region L_e, the strain-hardening region L_{sh} and the pullout cone region L_{pc}. The average elastic bond strength τ_{be} according to ACI 408 [36] is adopted here for the elastic region, while the frictional bond τ_{bf} according to the CEB Model Code [37] is assumed to apply within the strain-hardening region. In the pullout cone region, it is assumed that the acting bond is negligible.

For various levels of the applied end moment and using the results of M-φ analysis, the stress σ_s and strain ε_s of the reinforcing bar at the loaded end are first determined. Then, from equilibrium and applying the assumed bond distribution, variation of reinforcing bar stress $\sigma_s(x)$ along the embedment length is defined as shown in Fig. 8b, where σ_y is the yield strength of steel and σ_h is the stress at the end of the straight part of the rebar anchorage. Then, by assigning an appropriate constitutive material law for steel [38], strain distribution $\varepsilon_s(x)$ is determined, as shown in Fig. 8c, where ε_y and ε_{sh} are the steel strains at the onset of yielding and strain hardening, respectively, and ε_h is the steel strain at the end of the straight part of the anchorage. It is important to note that post-yield nonlinearity of the material constitutive law, i.e. strain hardening, should be taken into account because it affects significantly the final results [18].

Once $\varepsilon_s(x)$ is determined, slip of the reinforcement δ_{slip} can be calculated by integration along the anchorage length of the bar. In the case of hooked bars, local slip of the hook should be added. This can be evaluated by the force acting on the hook $P_h=A_b \cdot \sigma_h$, where A_b is the area of the anchored bar, and an appropriate hook force vs. hook slip relationship [39].

Upon determination of δ_{slip}, the respective fixed-end rotation can be calculated by Eq. (17), where $(d-x_c)$ is the distance between the bar and the neutral axis. The envelope M-θ_{slip} curve constructed by the various points of the afore-described methodology is then idealized by a bilinear relationship for the purposes of analysis.

$$\theta_{slip} = \frac{\delta_{slip}}{d - x_c} \tag{17}$$

After establishing the envelope curve, bond-slip hysteretic behaviour is determined by adopting the respective phenomenological model of Saatcioglu and Alsiwat [40]. Additional features have been introduced by the writers to prevent numerical instabilities resulting in the implementation of the specific model in the framework of nonlinear analysis [18].

6 Correlations with Experimental Results

The analytical model described in previous sections has been incorporated in the general finite element program for inelastic damage analysis of R/C structures IDARC2D (http://civil.eng.buffalo.edu/idarc2d50/). In the following, the proposed beam-column model is calibrated against experimental data from R/C column and frame specimens, which developed shear failures after yielding in flexure. Validation is extended, whenever possible, to individual deformation components in order to verify as thoroughly as feasible, all features of the model.

6.1 R/C bridge pier specimen HS2 by Ranzo & Priestley (2001)

Ranzo & Priestley [33] tested three thin-walled circular hollow columns. Herein, the specimen designated as HS2 is examined, which was designed to fail in shear after yielding in flexure. Its outer diameter was 1524mm and wall thickness 139mm. The ratio of the column shear span to the section outer diameter was equal to 2.5. The normalised applied compressive axial load was 0.05. Longitudinal reinforcement ratio was 2.3% and the volumetric ratio of transverse reinforcement 0.35%. Concrete strength was 40MPa and yield strengths of longitudinal and transverse reinforcement were 450MPa and 635MPa, respectively. Lateral actions were applied in the push and pull direction of the column for increasing levels of displacement ductility μ_Δ with three repeated cycles at each μ_Δ. For this specimen, initial shear strength is predicted equal to 1930kN.

Fig. 9 shows the experimental and analytical lateral load vs. total displacement response of the specimen. The analytical model captures accurately the initial stiffness, lateral strength and hysteretic response of the R/C member. More importantly, the proposed model is able to predict reasonably well the tip displacement at which onset of shear failure and consequent strength degradation is developed.

This can be seen also in Fig. 10a, which compares shear strength given by Eq. (6) and acting shear force as a function of the end section curvature demand. Initially, shear capacity exceeds significantly shear demand. However, due to inelastic curvature development, at the end of the analysis shear demand reaches shear capacity marking the onset of stirrup yielding. It is worth reporting that maximum curvatures predicted by the analytical model (0.019rad/m and 0.025rad/m in positive and negative bending respectively) correlate sufficiently with the measured ones inside the plastic hinge region (approx. 0.02rad/m) [33].

Fig. 10b illustrates shear strain distribution of the R/C column as predicted by the proposed shear sub-element for various levels of increasing μ_Δ. For μ_Δ=1.0, shear strains remain constant along the height of the member. After $\mu_\Delta \geq 1.5$, a double effect is noted: First, shear strains in the inelastic zone increase more rapidly and tend to differ substantially from the ones in the intermediate part of the element due to shear-flexure interaction effect and consequent yielding of transverse reinforcement. Second, the length of the inelastic zone increases following expansion of flexural yielding towards the mid-span. By this combined effect, gradual spread of inelastic shear deformations is appropriately captured by the model.

Figs 11a and 11b present shear hysteretic response resulting by the proposed model inside and outside the plastic hinge region. It can be seen that while acting shear remains the same in both parts of the element, shear strains become significantly higher inside the inelastic zone. At the onset of shear failure, occurring inside the plastic hinge, shear deformations are predicted equal to 0.3% and 1.3% outside and inside the inelastic zone, respectively. Both of these values are in good agreement with the experimental results (approx. 0.3% and 1.2% respectively) [33].

6.2 R/C beam specimen R5 by Ma et al. (1976)

Ma et al. [1] tested nine cantilever beams, representing half scale models of the lower story of a 20-storey ductile moment-resisting R/C office building. Herein, the specimen designated as R5 is examined. Shear span ratio was equal to 2.41. Longitudinal reinforcement consisted of 4 top and 4 bottom 19mm bars, while volumetric ratio of transverse reinforcement was set equal to 0.31%. Concrete strength was 31.5MPa and yield strengths of longitudinal and transverse reinforcement were 452MPa and 413MPa, respectively. The specimen was subjected to a cyclic concentrated load at the free end. For this specimen, initial shear strength is predicted equal to 314kN.

Fig. 12 presents lateral load vs. lateral displacement response as derived by the proposed model and as recorded experimentally. It can be seen that the analytical model reproduces sufficiently the experimental initial stiffness, lateral load capacity, and unloading stiffness. Reloading stiffness is predicted well during the early phases of inelastic response. However, as displacement demand increases, the pinching effect is underestimated leading to a small overestimation of the energy dissipation capacity of the member. It is pointed out that the displacement level at which shear failure is predicted by the analytical model correlates sufficiently well with the onset of serious shear strength degradation in the experimental response ($\mu_{\Delta}\approx4$).

Fig. 13a compares shear strength given by Eq. (6) and acting shear force as a function of the end section curvature demand. Initially, shear capacity exceeds significantly shear demand. However, due to inelastic curvature development, at the end of the analysis shear demand reaches shear capacity marking the onset of stirrup yielding. Maximum curvature demand is well predicted (experiment 0.11rad/m and prediction 0.12rad/m).

Fig. 13b shows moment vs. fixed-end rotation hysteretic response caused by anchorage slippage as derived by the analytical model described in this study. Maximum rotation is predicted equal to 0.007rad in both directions. This hysteretic relationship is not reported in [1] for the specimen under examination.

Fig. 13c illustrates shear hysteretic response inside the plastic hinge region as predicted by the analytical model. It is obvious that this relationship is characterised by intense pinching effect following the hysteretic model proposed in [4]. The predicted behaviour matches adequately the experimental response with slight underestimation of the observed pinching effect [1]. This is the reason for underestimating pinching effect in the total displacement response (Fig. 12). Shear deformation at onset of shear failure is calculated equal to 0.043 and is in close agreement with the experimental evidence as shown in Table 1.

In Fig. 13c, V-γ envelope is also included without considering shear-flexure interaction. Initially, the initial envelope determines shear hysteretic response. Nevertheless, as soon as $\mu_{\varphi}>3$, shear deformations increase more rapidly, due to interaction with flexure, and shear hysteresis separates from the skeleton curve. After stirrup yielding, occurring for $\gamma\approx4‰$, shear rigidity becomes close to

zero and V-γ skeleton curve including shear-flexure interaction continues in parallel with the initial envelope.

In Fig. 13d, variation of displacement components with μ_Δ is presented as derived by the proposed model and experimental recordings. It can be seen that the analytical and experimental displacement patterns are in close agreement. Although shear demand after flexural yielding remains almost constant, analytically derived shear displacement increases significantly due to modelling interaction with flexure and subsequent stirrup yielding.

6.3 R/C frame specimen by Duong et al. (2007)

This single-bay, two-storey frame (Fig. 14a) was tested by Duong et al. [41] at University of Toronto. The frame was subjected to a single loading cycle. During the experiment, a lateral load was applied to the second storey beam in a displacement controlled mode, while two constant axial loads were applied throughout the testing procedure to simulate the axial load effects of upper storeys (Fig. 14a). During loading sequence, the two beams of the frame experienced significant shear damage (close to shear failure) following flexural yielding at their ends [41].

The finite element model applied herein for the inelastic cyclic static analysis of the frame is also shown in Fig. (14a). It consists of 4 column elements and 2 beam elements (one for each column and beam). Hence, the number of finite elements applied is minimal, ensuring high computational efficiency of the numerical model. The columns are assumed to be fixed at the foundation. Rigid arms are employed to model the joints of the frame.

Figs (14b), (14c) compare the experimental and analytical top displacement and base shear responses obtained by three different versions of the proposed model. **Model F** includes only flexural deformations. **Model FB** combines flexural and anchorage slip deformations. Finally, **Model FSB**, which is the one proposed in this study, incorporates all three types of deformations (flexure, shear, anchorage slip).

As shown in Fig. (14b), model FSB follows closely the experimental behaviour over the entire range of response. Slight underestimation of the frame lateral stiffness takes place at the early stages of loading. This is due to the fact that flexural response prior to cracking is not modelled in this study. However, the following gradual decrease of frame stiffness is sufficiently captured by the analytical model. At maximum displacement, the analytical model slightly overestimates lateral strength (having a calculated-to-observed ratio of 1.10 in both directions). Furthermore, the analytical model predicts correctly that both beams develop shear failures after yielding in flexure.

On the other hand, models F and FB considerably overestimate both stiffness and strength, and consequently the ability of the examined frame to dissipate hysteretic energy. For the F model, the calculated-to-observed ratio for strength is 1.30 and 1.23, in the positive and negative direction respectively. The prediction is improved with inclusion of anchorage slip effect in the FB model and the aforementioned ratios become 1.19 and 1.22.

Fig. (14e) presents the pushover curves obtained by the different finite element models. It can be seen that models F and FB overestimate stiffness, strength, and displacement capacity. At the end of the analysis, the F and FB models overestimate strength by 38% and 37% respectively. The same models overestimate displacement capacity by 52% and 358% accordingly. Both models erroneously predict flexural failure at the base of the frame.

The FSB model predicts correctly that shear failure is developed after yielding in flexure. However, inclusion of shear-flexure interaction effect and degradation of shear strength with curvature ductility demand affects substantially the displacement capacity predicted by this analytical model. When shear-flexure interaction is considered, ultimate displacement capacity is found to be 46mm, which is very close to the 44.7mm recorded experimentally. On the other hand, if shear-flexure interaction is ignored, displacement capacity is overestimated by 228%.

Finally, Figs (14e) and (14f) present shear force vs. shear strain hysteresis loops predicted by the FSB analytical model inside and outside the plastic hinge regions for the 1st storey beam of the frame under cyclic loading. It can be seen that, due to shear-flexure interaction effect and consequent stirrup yielding, shear strains are predicted significantly higher inside than outside the plastic hinges (1.26% instead of 0.53%), while shear force remains constant along this RC member.

6.4 R/C frame specimen 1 by Elwood & Moehle (2008)

This half-scale frame specimen was constructed and tested on the shaking table at the University of California, Berkeley [42]. It comprised three columns interconnected at the top by a 1.5m wide beam and supported at the bottom on footings (Fig. 15a). The columns supported a total mass of 31t.

To represent R/C columns typical of 1960s construction in the Western United States, the central column was constructed with light transverse reinforcement having 90^{o} hooks. The outside columns were detailed with closely spaced spiral reinforcement to ensure ductile response and to provide support for gravity loads after shear failure of the central column.

The specimen was subjected to one horizontal component of the ground motion recorded at Viña del Mar during the 1985 Chile earthquake (SE32 component). The normalised axial load in the central column was 0.10. During testing, the central column experienced a loss of lateral load capacity, due to apparent shear failure at its top, during a negative displacement cycle at approximately 17.6sec [42].

The finite element model applied herein for the inelastic response-history analysis of the frame is shown in Fig. (15a). It consists of 3 column elements and 2 beam elements (one for each member). Hence, the number of finite elements required is minimal, ensuring low computational cost.

The columns are assumed to be fixed at the foundation. Rigid arms are employed to model the joints of the frame. Rayleigh model is used for viscous damping. The equivalent viscous damping is set equal to 2% of critical for the fundamental vibration mode. The mass is assumed lumped at the top of the frame. In the following, for the calculation of the central column shear strength, the

contribution of the stirrups is reduced by half to take into account their inadequate anchorage (90^o hooks). Hence, initial shear strength is determined equal to 115kN for this member.

Figs (15b), (15c) compare the experimental and analytical top displacement and base shear respectively response histories between t=10sec and onset of shear failure. The first 10 seconds are omitted so that the critical duration of response can be more clearly observed. It is evident that the analytical model predicts closely the experimental response up to the onset of shear failure of the central column.

The same conclusion can be drawn in Fig. (15d), which presents the comparison between the experimental and analytical hysteresis loops for the frame, up to onset of shear failure. It is apparent that the analytical model captures satisfactorily the initial frame stiffness, maximum shear capacity and the displacement corresponding to onset of shear failure.

Finally, Fig. (15e) compares the pushover curves obtained by four different versions of the proposed finite element model and the experimental response. The comparison is shown in the negative displacement direction because in this direction shear failure was detected.

Model F, which tackles only flexural deformations, significantly overestimates initial frame stiffness and underestimates displacement at failure. In particular, this model predicts erroneously flexural failure at the base of the central column at a 20mm lateral displacement.

Model FS which combines flexure and shear, predicts correctly the development of shear failure at the top of central column. However, it significantly overestimates initial lateral stiffness and underestimates displacement capacity at onset of shear failure (27mm instead of 51mm).

Model FB, which includes flexural and anchorage slip deformations, provides better estimates than the two previous models. However, it overestimates initial stiffness after base shear exceeds 150kN (onset of shear cracking) and underestimates considerably displacement at onset of lateral failure (37mm instead of 51mm). Moreover, a flexural failure at the base of the central column is falsely predicted.

The best estimations are provided by the FSB model which incorporates all types of deformations. Envelope stiffness is closely captured until maximum response. Additionally, this model predicts correctly a shear failure at the top of the central column at a 47mm displacement, which is quite close to the experimental value.

7 Summary and Conclusions

A new beam-column finite element for inelastic analysis of R/C planar frame structures was introduced and verified against experimental results. The model is of the phenomenological type and is developed using the flexibility approach. It consists of three individual sub-elements connected in series and accounting for member flexural, shear, and anchorage slip response.

The flexural sub-element is used for modelling flexural behaviour before and after yielding of longitudinal reinforcement. By adopting a spread inelasticity formulation, it is able to account for variation of section stiffness along the R/C member.

Shear flexibility is modelled explicitly via the shear sub-element. This sub-element is capable of reproducing gradual spread of inelastic shear deformations, developed in plastic hinges, from the member ends to the midspan, a feature that cannot be found in any of the existing models. This is achieved by determining the length and stiffness of its inelastic zones through a dual interaction procedure with the flexural sub-element.

Shear stiffness is defined by the respective primary curve and the empirical hysteretic model described in [4]. Initially, shear skeleton response is modelled without shear-flexure interaction. This envelope curve is appropriate for modelling shear response outside the plastic hinge regions. Herein, new empirical formulae are proposed for evaluating shear distortion at onset of stirrup yielding and shear failure. Then, by developing a new analytical procedure, which combines the truss analogy approach and the shear strength model by Priestley et al. [5], the V-γ envelope within plastic hinge regions is determined. In this way, shear strength degradation and rapid increase of inelastic shear deformations following flexural yielding are modelled simultaneously and in a rational manner.

Fixed-end rotations caused by anchorage slippage are modelled by nonlinear rotational springs. M-θ_{slip} skeleton curve is determined by a simplified procedure assuming constant, uniform bond stress distribution along the elastic and inelastic part of the anchorage length. Post-yield nonlinearity of the constitutive law for steel, i.e. strain hardening, is taken into consideration. Anchorage slip hysteretic relationship is modelled following the phenomenological approach described in [40].

The proposed analytical model was implemented in the finite element program IDARC and was validated against experimental results from R/C column specimens failing in shear subsequent to yielding in flexure. Model calibration was not restricted to total response parameters, but also encompassed individual deformation and displacement components. In all cases, sufficient agreement was achieved with the experimental observations.

The developed beam-column model represents a complete proposal for modelling inelastic response of R/C members since all deformations mechanisms (flexure, shear, anchorage slip), as well as their interaction and gradual development, are duly taken into consideration. At the same time, the numerical formulation remains robust and requires minimum computational effort. Hence, it is believed that the proposed finite element constitutes an efficient analytical tool for seismic assessment of R/C structures.

References

[1] Ma SM, Bertero VV, Popov EP. Experimental and analytical studies on hysteretic behaviour of R/C rectangular and T-beam. Report EERC 76-2. Berkeley: University California Berkeley; 1976.

[2] Oesterle RG, Fiorato AE, Aristizabal-Ochoa JD. Hysteretic response of reinforced concrete structural walls. In: Proceedings of ACISP-63: Reinforced Concrete Structures subjected to Wind and Earthquake Forces, Detroit; 1980.

[3] Saatcioglu M, Ozcebe G, Response of reinforced concrete columns to simulated seismic loading. ACI Structural Journal 1989; 86(1): 3-12.

[4] Ozcebe G, Saatcioglu M. Hysteretic shear model for reinforced concrete members. Journal of Structural Engineering 1989; 115(1): 132-48.

[5] Priestley MJN, Seible F, Verma R, Xiao Y. Seismic shear strength of reinforced concrete columns. Report No. SSRP-93/06. California: University of San Diego; 1993.

[6] Biskinis D, Roupakias G, Fardis MN. Degradation of shear strength of R/C members with inelastic cyclic displacements. ACI Structural Journal 2004; 101(6): 773-83.

[7] Sezen H, Moehle JP. Shear strength model for lightly reinforced concrete columns. Journal of Structural Engineering 2004; 130(11): 1692-703.

[8] Takayanagi T, Derecho AT, Gorley WG. Analysis of inelastic shear deformation effects in reinforced concrete structural wall systems. In: Proceedings of CSCE-ASCE-ACI-CEB International Symposium, University of Waterloo, Ontario, Canada; 1979.

[9] Filippou FC, D' Ambrisi A, Issa A. Nonlinear static and dynamic analysis of RC subassemblages. Report EERC 92-08. California: Univ. California Berkeley; 1992.

[10] Ricles JM, Yang YS, Priestley MJN. Modelling nonductile R/C columns for seismic analysis of bridges. Journal of Structural Engineering 1998; 124(4): 415-25.

[11] Pincheira J, Dotiwala F, Souza J. Seismic analysis of older reinforced concrete columns. Earthquake Spectra 1999; 15(2): 245-72.

[12] Petrangeli M, Pinto P, Ciampi V. Fibre element for cyclic bending and shear or R/C structures. I: Theory. Journal of Engineering Mechanics 1999; 125(9): 994-1001.

[13] Marini A, Spacone E. Analysis of reinforced concrete elements including shear effects. ACI Structural Journal 2006; 103(5): 645-55.

[14] Soleimani D, Popov EP, Bertero VV. Nonlinear beam model for R/C frame analysis. In: Proceedings of Seventh Conference on Electronic Computation, St. Louis, Misouri; 1979.

[15] Valles RE, Reinhorn AM, Kunnath SK, Li C, Madan A. IDARC2D Version 4.0: A program for the inelastic damage analysis of buildings. Technical Report NCEER-96-0010. New York: State University of New York at Buffalo; 1996.

[16] Mergos PE, Kappos AJ. A distributed shear and flexural flexibility model with shear-flexure interaction for R/C members subjected to seismic loading. Earthquake Engineering and Structural Dynamics 2008; 37(12): 1349-70.

[17] Mergos PE, Kappos AJ. Seismic damage analysis including inelastic shear-flexure interaction. Bulletin of Earthquake Engineering 2010; 8(1): 27-46.

[18] Mergos PE. Assessment of seismic behaviour of existing RC structures. PhD Thesis. Greece: Aristotle University of Thessaloniki; 2011.

[19] Vecchio FJ, Collins MP. The modified compression field theory for reinforced concrete elements subjected to shear. ACI Structural Journal 1986; 83(2): 219-31.

[20] Priestley MJN, Seible F, Calvi GM. Seismic design and retrofit of bridges. New York: Wiley; 1996.

[21] Sivaselvan MV, Reinhorn AM. Hysteretic model for cyclic behaviour of deteriorating inelastic structures. Technical report MCEER-99-0018. New York: State Univ. of New York at Buffalo; 1999.

[22] Clough RW. Effect of stiffness degradation on earthquake ductility requirements. Structures and Materials Research Report No 66-16. California: Univ. of California Berkeley; 1966.

[23] Park R, Paulay T. Reinforced concrete structures. New York: Wiley; 1975.

[24] Aboutaha R, Engelhardt D, Jirsa J, Kreger E. Rehabilitation of shear critical concrete columns by use of rectangular steel jackets. ACI Structural Journal 1999; 96(1)**:** 68-77.

[25] Lam SSE, Wu B, Wong YL, Wang ZY, Liu ZQ, Li CS. Drift capacity of rectangular reinforced concrete columns with low lateral confinement and high-axial load. Journal of Structural Engineering 2003; 129(6): 733-42.

[26] Sezen H. Seismic behaviour and modelling of R/C building columns. PhD Thesis. California: University of California Berkeley; 2002.

[27] Arakawa T, Arai Y, Egashira K, Fujita Y. Effects of the rate of cyclic loading on the load carrying capacity and inelastic behaviour of R/C columns. Transactions of the Japan Concrete Institute 1982; 4: 485-92.

[28] Umehara H, Jirsa JO. Shear strength and deterioration of short R/C columns under cyclic deformations. PMFSEL Report No. 82-3. Texas: University of Texas, Austin; 1982.

[29] Bett B, Klinger R, Jirsa JO. Behaviour of strengthened and repaired R/C columns under cyclic deformations. PMFSEL Report No. 85-3. Texas: University of Texas, Austin; 1985.

[30] Garstka B. Investigations on resistance and damage behaviour of RC linear elements considering shear effects under cyclic nonlinear loading. Report Nr. 93-2. Germany: Institut für Konstruktiven Ingenieurbau, Ruhr-Universität Bochum; 1993.

[31] Yoshimura M, Takaine Y, Nakamura T. Collapse drift of R/C columns. In: Proceedings of 5th US-Japan Workshop on Performance Based Earthquake Engineering Methodology for R/C Building Structures: 239-254; 2003.

[32] Kowalsky MJ, Priestley MJN. Shear behaviour of lightweight concrete columns under seismic conditions. Report No. SSRP-95/10, California: University of San Diego; 1995.

[33] Ranzo G, Priestley MJN. Seismic Performance of Circular Hollow Columns Subjected to High Shear. Report No. SSRP-2001/01. California: University of San Diego; 2001.

[34] Alsiwat JM, Saatcioglu M. Reinforcement anchorage slip under monotonic loading. Journal of Structural Engineering 1992; 118(9): 2421-38.

[35] Lowes L, Altoontash A. Modeling Reinforced Concrete Beam-Column Joints Subjected to Seismic Loading. Journal of Structural Engineering 2003; 129(12): 1686-97.

[36] ACI Committee 408. Bond and development of straight reinforcement in tension. American Concrete Institute: Farmington Hills; 2003.

[37] CEB Bulletin No. 213/214. CEB-FIP model code 90; 1993.

[38] Park R, Sampson RA. Ductility of reinforced concrete column sections in seismic design. ACI Structural Journal 1972; 69(9): 543-51.

[39] Soroushian P, Kienuwa O, Nagi M, Rojas M. Pullout behaviour of hooked bars in exterior beam-column connections. ACI Structural Journal 1988; 85(3): 269-76.

[40] Saatcioglu M, Alsiwat J. Hysteretic behaviour of anchorage slip in R/C members. Journal of Structural Engineering 1992; 118(9): 2439-58.

[41] Duong KV, Sheikh FJ, Vecchio F. Seismic behaviour of shear critical reinforced concrete frame: Experimental Investigation. ACI Structural Journal 2007; 104(3): 304-13.

[42] Elwood K, Moehle JP. Dynamic collapse analysis for a reinforced concrete frame sustaining shear and axial failures. Earthquake Engineering and Structural Dynamics 2008; 37 (7): 991-1012.

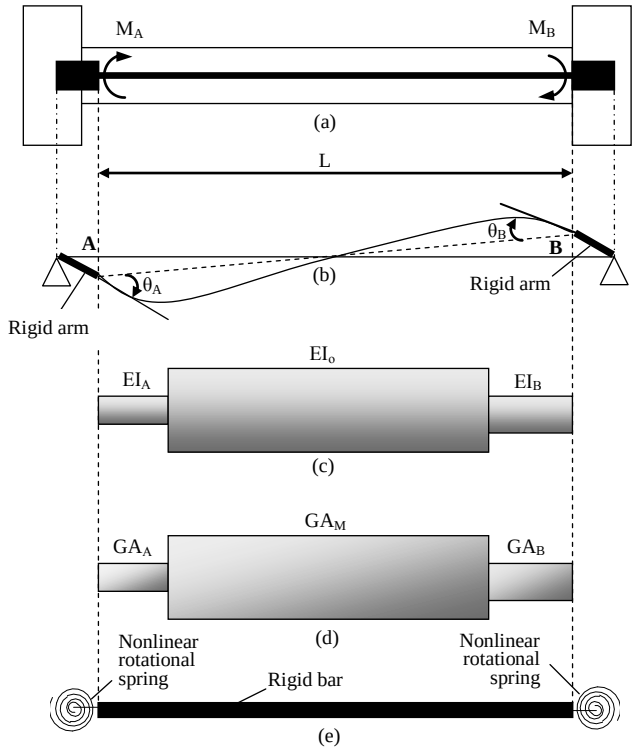

Figure 1: Proposed finite element model: a) geometry of R/C member; b) beam-column finite element with rigid arms; c) flexural sub-element; d) shear sub-element, e) anchorage slip sub-element.

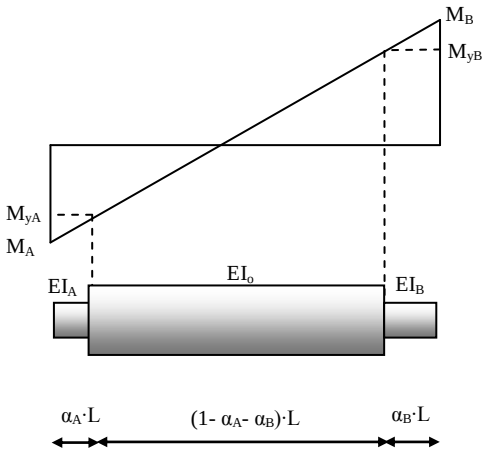

Figure 2: Flexural spread inelasticity model.

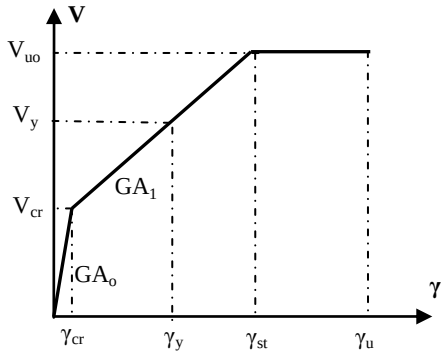

Figure 3: Initial V-γ primary curve.

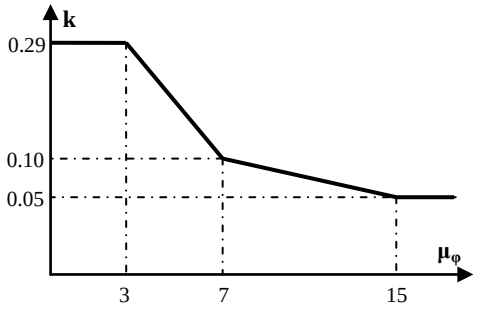

Figure 4: Relationship between curvature ductility demand and strength of concrete shear resisting mechanisms.

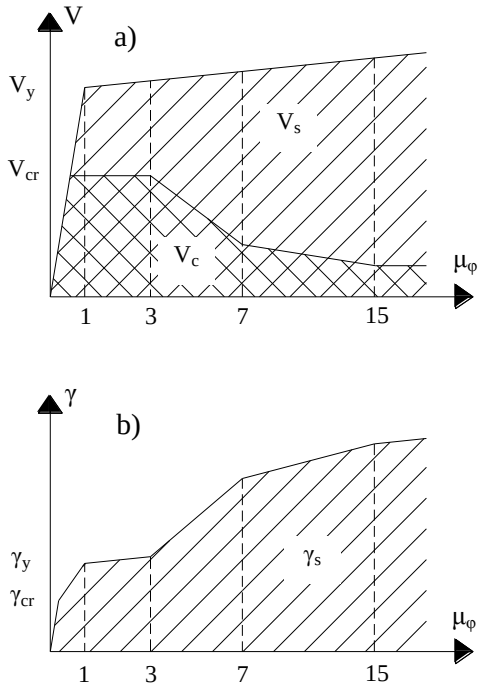

Figure 5: Variation of a) shear resisting mechanisms; b) shear strain after shear cracking with curvature ductility demand in plastic hinge regions of R/C members.

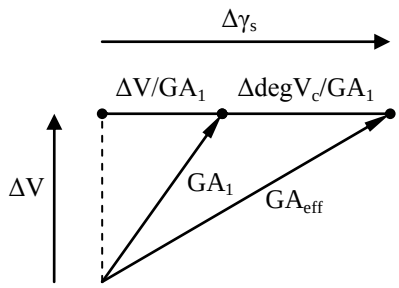

Figure 6: Definition of GA_{eff}.

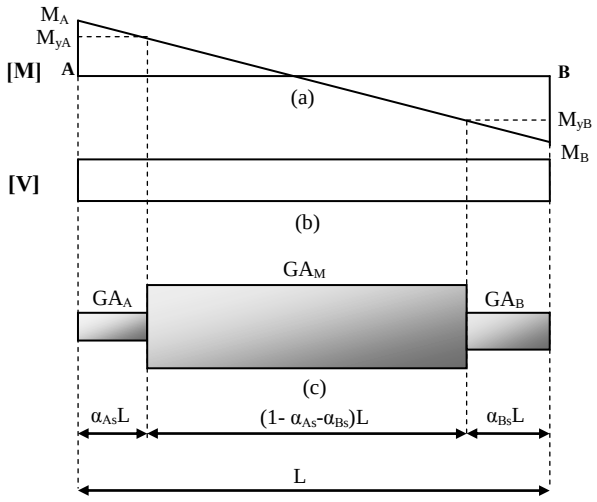

Figure 7: Shear spread inelasticity model: a) moment diagram; b) shear diagram; c) shear spread model.

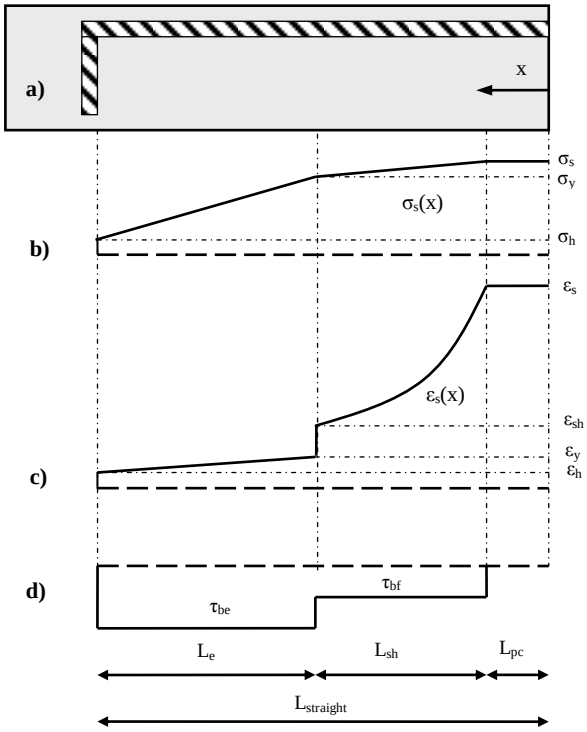

Figure 8: a) Reinforcing bar with 90^{o} hook embedded in concrete; b) steel stress distribution; c) strain distribution; d) bond stress distribution.

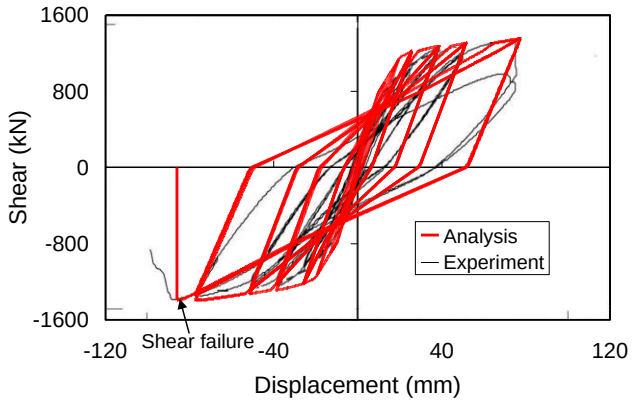

Figure 9: Lateral load vs. total displacement response for specimen HS2 (Ranzo & Priestley 2001).

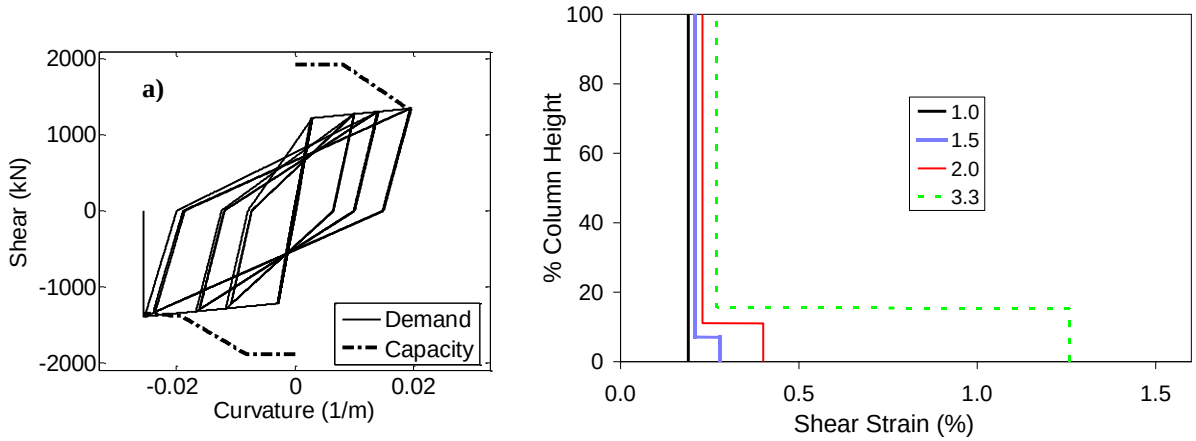

Figure 10: a) Shear demand and capacity as a function of the end section curvature demand; b) shear strain distribution for increasing displacement ductility demands.

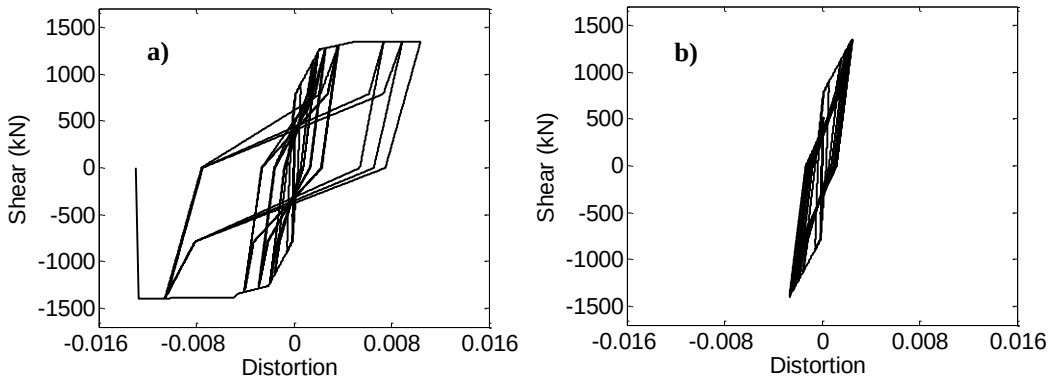

Figure 11: Predicted shear hysteretic response a) inside; b) outside plastic hinge region.

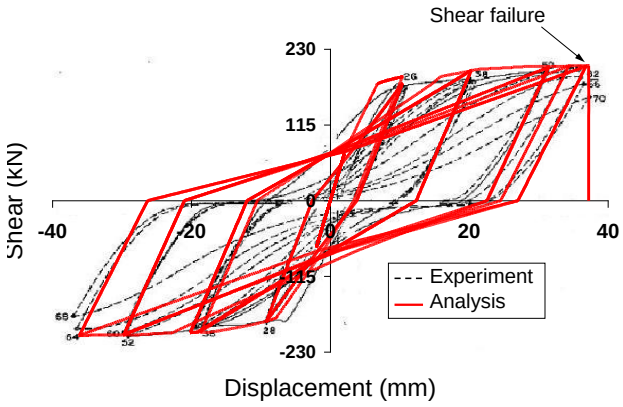

Figure 12: Lateral load vs. total displacement response for specimen R5 (Ma et al. 1976).

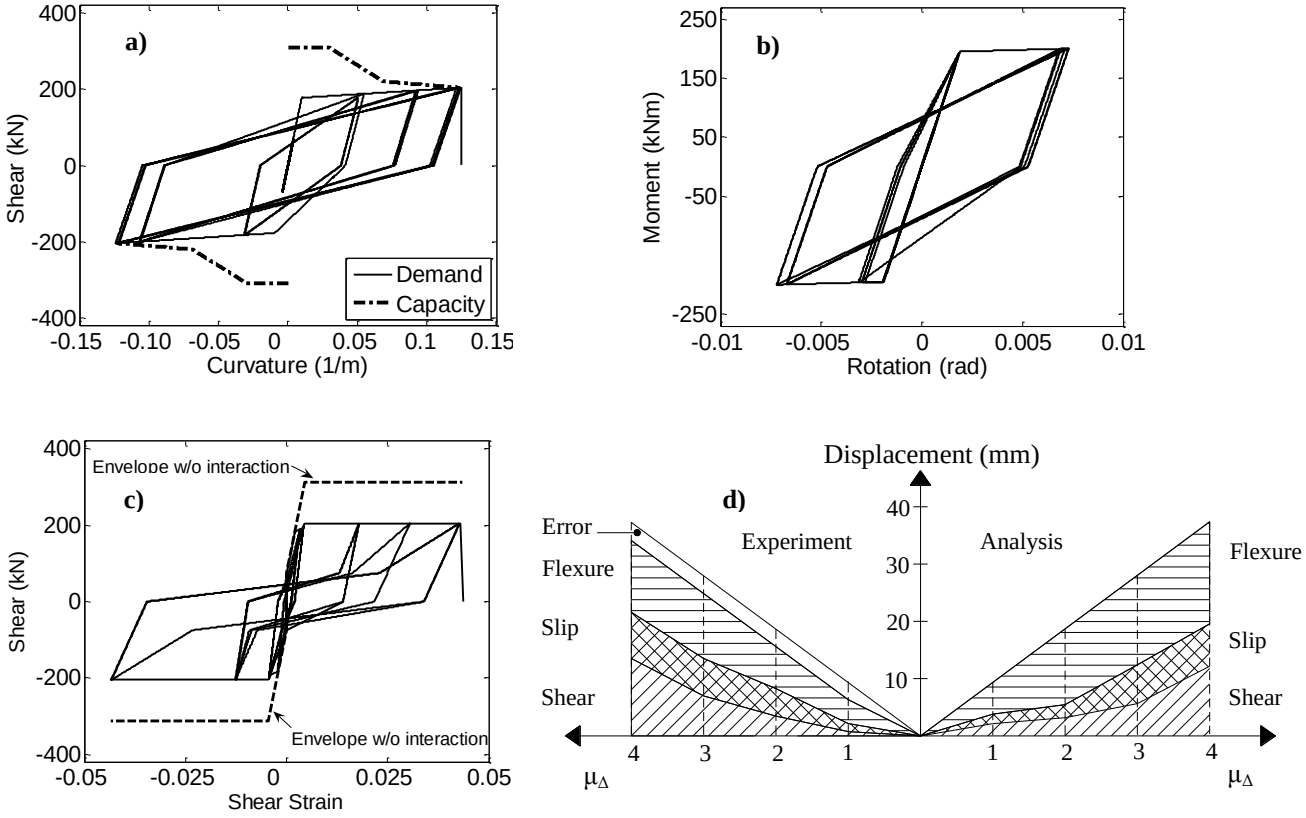

Figure 13: a) Shear demand and capacity as a function of the end section curvature demand; b) analytical M-θ_{slip} hysteresis; c) analytical V-γ relationship inside the plastic hinge region and d) variation of member displacement components with μ_Δ predicted by the analytical model and measured experimentally.

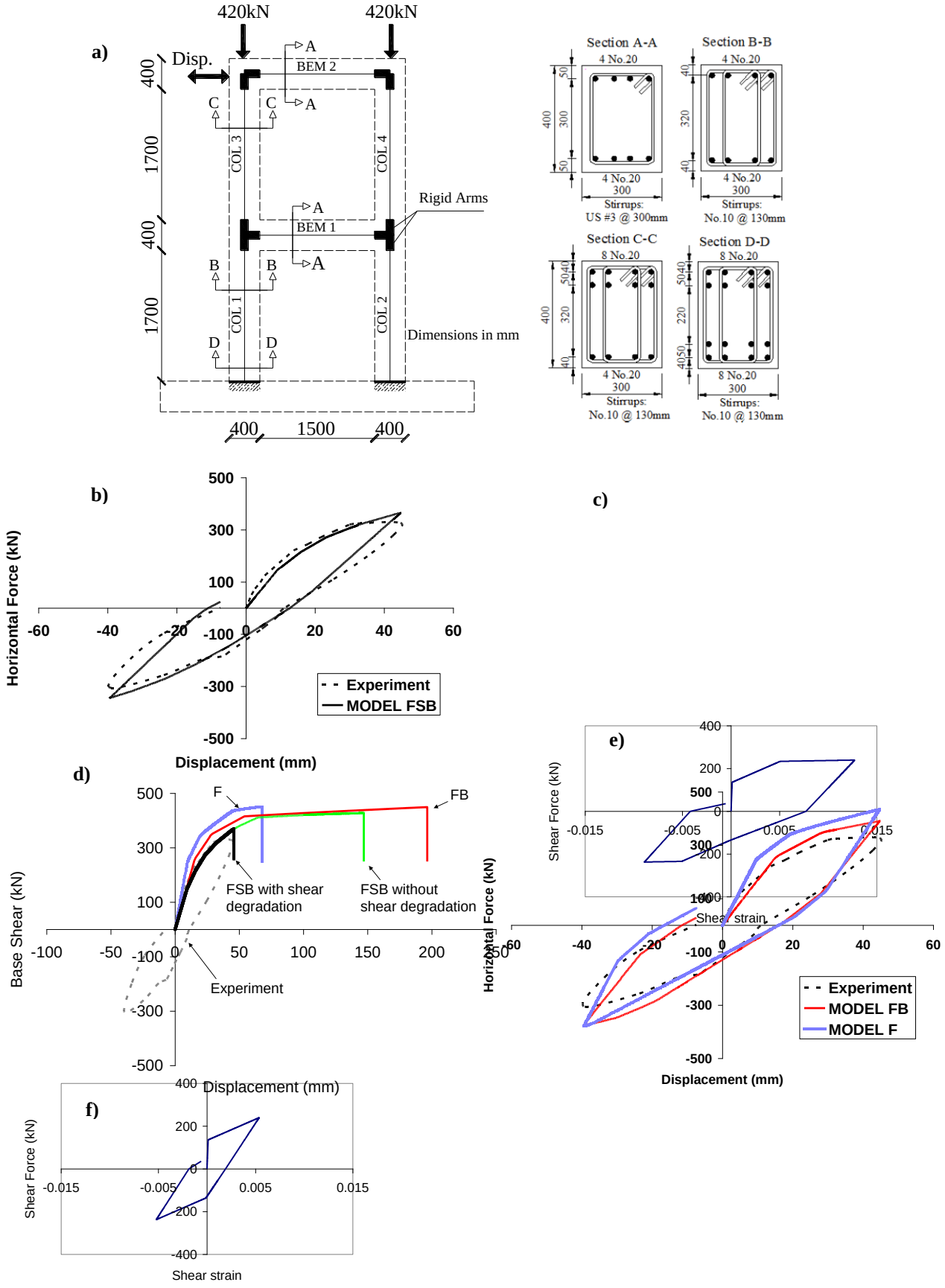

Figure 14: a) Duong et al. frame specimen layout and corresponding finite element model; (b) base shear vs. top displacement prediction by FSB model; c) base shear vs. top displacement predictions by F and FB models; d) pushover curves from different finite element models; e) first

storey beam shear force vs. shear strain response inside plastic hinges; f) first storey beam shear force vs. shear strain response outside plastic hinges.

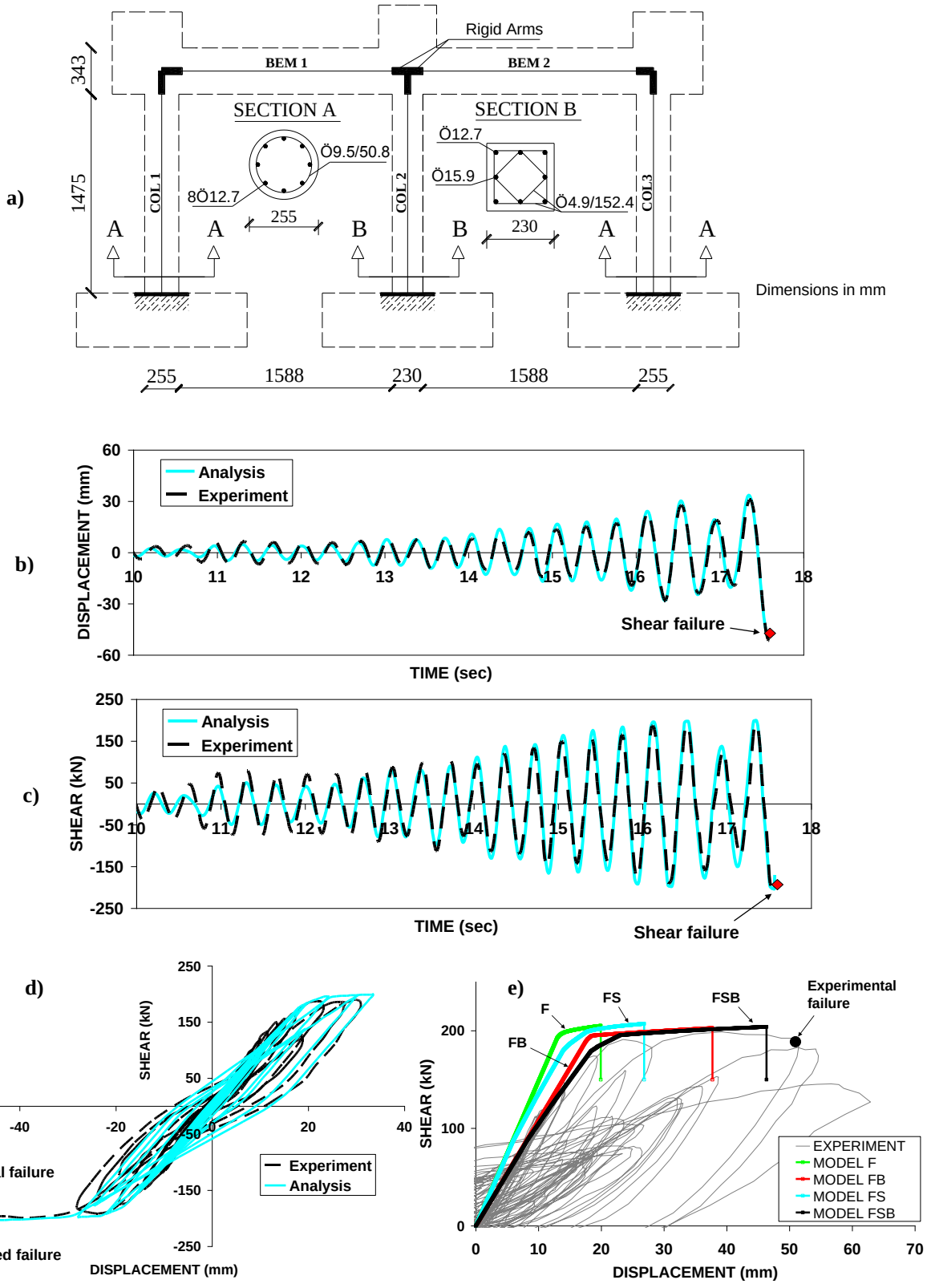

Figure 15: a) Elwood & Moehle frame specimen 1 layout and corresponding finite element model; (b) displacement time history; c) base shear time history; d) frame hysteresis; e) pushover curves from F, FB, FS and FSB finite element models and comparison with the experimental response.

Ref.	Specimen	L_s/h	v	ω_κ (%)	γ_{st} (‰)		γ_u (‰)	
					Experiment	Prediction	Experiment	Prediction
[1]	R5	2.41	0.00	8.03		4.1	40.0	43.0
[1]	R6	3.91	0.00	8.13		3.4	38.0	37.2
[4]	U1	2.86	0.00	3.22		3.6	21.1	20.1
[5]	R3A	2.00	0.06	1.15	3.3	3.7	3.3	6.4
[5]	C5A	2.00	0.06	0.74	5.4	3.7	5.4	5.6
[25]	X2	1.50	0.40	0.49	2.7	2.9	2.7	2.9
[26]	2CLD12	3.22	0.15	3.93	2.7	3.0	14.0	11.8
[26]	2CHD12	3.22	0.61	3.93	1.0	1.3	3.0	1.3
[26]	2CLD12M	3.22	0.15	3.93	3.3	3.0	9.0	11.8
[27]	OA2	1.25	0.18	1.70	4.6*	4.3	4.6*	4.3
[28]	CUS	1.11	0.16	3.28	9.0*	7.5	9.0*	7.5
[28]	2CUS	1.11	0.27	2.72	7.1*	6.8	7.1*	6.8
[29]	No 1-1	1.50	0.10	2.08	5.1*	6.2	5.1*	7.1
[24]	SC9	1.33	0.00	1.92	5.5*	6.9	5.5*	8.0
[24]	SC3	2.67	0.00	1.75	3.4*	2.9	12.9*	11.4
[30]	SBV1	1.67	0.00	3.07		7.7	18.0	18.5
[30]	SBV2	2.20	0.00	3.07		5.3	22.0	21.9
[30]	SBV3	2.50	0.00	3.07		3.9	26.0	21.0
[31]	No. 1	2.00	0.20	2.41	2.9*	3.8	2.9*	5.7
[31]	No. 3	2.00	0.30	1.20	3.3*	3.3	3.3*	3.3
[31]	No. 4	2.00	0.35	2.41	2.5*	3.1	2.5*	3.1
[32]	SL1	2.00	0.04	0.47	3.7	3.2	3.7	4.5
[32]	SL2	2.00	0.04	2.50		5.0	17.0	13.6
[33]	HS2	2.50	0.05	0.84		5.0	12.0	12.6
[33]	HS3	2.50	0.15	0.96		3.9	5.0	7.3

Table 1: Experimental and predicted values for γ_{st} and γ_u

A Kappos

From: ees.engstruct.e.195ff4.b6fdeaef@eesmail.elsevier.com on behalf of Herbert Mang [Herbert.Mang@tuwien.ac.at]
Sent: Τετάρτη, 23 Μαΐου 2012 11:49 πμ
To: ajkap@civil.auth.gr
Subject: Your Submission

Ms. Ref. No.: ENGSTRUCT-D-11-00778
Title: A gradual spread inelasticity model for R/C beam-columns, accounting for flexure, shear and anchorage slip
Engineering Structures

Dear Prof. Kappos,

The paper "A gradual spread inelasticity model for R/C beam-columns, accounting for flexure, shear and anchorage slip" has been accepted for publication in Engineering Structures.

Proofs and a copyright form will be send directly to you by Elsevier prior to publication.

Thank you for choosing Engineering Structures.

With best regards,

Herbert A. Mang
Editor
Engineering Structures